Chapter 5
Memristive Biosensors for Ultrasensitive Diagnostics and Therapeutics

Ioulia Tzouvadaki, Giovanni De Micheli and Sandro Carrara

Abstract The coupling of memristive effect with biological interactions results in innovative nanobiosensors with high performance in both diagnostics and therapeutics. Silicon nanowire arrays exhibiting a memristive electrical response are acquired through a top-down nanofabrication process. Surface treatments implementing sophisticated bio-functionalization strategies and adopting suitably selected biological materials give rise to the *memristive biosensors*. The particular electrical response of these novel biosensors leverages the modification of the hysteretic properties exhibited by the memristive effect before and after the bio-modification, to achieve an efficient detection of biological processes. *Memristive biosensors* successfully address the issue of the early detection of cancer biomarkers providing a new technology for high performance, ultrasensitive, label-free electrochemical sensing platforms. They also offer the capability of detecting extremely small traces of cancer biomarkers, as well as effective screening and continuous monitoring of therapeutic compounds in full human serum bringing novelty and solutions in the medical practice, especially in the field of personalized medicine.

5.1 Challenges in Biosensing

Even nowadays, the medical devices still face several limitations concerning rapid, reliable, and ultrasensitive sensing of biomarkers from a minimized volume of clinical samples. In particular, cancer diagnosis usually involves uncomfortable medical tests, long waiting times for the results of the medical assessment, nonetheless, risking to obtain an uncertain medical outcome. An other very important aspect is the

I. Tzouvadaki (✉) · G. De Micheli · S. Carrara
Integrated Systems Laboratory, EPFL, Lausanne, Switzerland
e-mail: ioulia.tzouvadaki@alumni.epfl.ch

G. De Micheli
e-mail: giovanni.demicheli@epfl.ch

S. Carrara
e-mail: sandro.carrara@epfl.ch

diagnosis of the disease at early stages, when suitable therapy decision-making can be taken into consideration for treatment, giving higher probability of success at the beginning of the disease. However, the diagnostic tools still lack the level of resolution needed for the detection of biomarkers at the early stages of the disease. Moreover, the clinical practice still lacks analytical methods for efficient, ultrasensitive monitoring of therapeutic compounds. Reliable, low-cost, and accessible therapeutic compound monitoring systems for individualized health care, and especially for treatment of malignant diseases, such as cancer and AIDS consist of a very important aspect in medical practice. These requirements are even more highlighted for drugs demonstrating a very narrow therapeutic window which is also depicted at low concentrations. Moreover, different patients may present different responses to the very same dose of drug, giving different therapeutic response from what expected.

Therefore, the realization of novel ultrasensitive nanobiosensors for the direct and label-free detection of chemical and biological species which present high reliability, robustness, and the advantage of a quick data acquisition may achieve optimum sensing output in both diagnostics and therapeutics fields, opening to early diagnostics and a treatment with higher efficacy and lower side effects for patients.

Nanostructure-based sensors are considered as a highly promising strategy to address the issues of sensitivity and limits of detection for both diagnostics and therapeutics and may allow the integration of the sensors in portable devices including microfluidics and electronics for robust, flexible, and automatized clinical applications. Silicon (Si) nanowires with their unique properties such as the high surface-to-volume ratio and the size comparable to biomolecules, and combined with the specificity of immune-sensing techniques, may provide optimum biosensing platforms [1].

In addition, although the fact that memristive effect has already been introduced in many different applications, very few of the implementations are dedicated for bio-detection. Carrara et al. [2] demonstrated for the first time the potential use of memristive effects in nanostructured devices for biosensing applications. Therefore, the aspect of memristive phenomena is expanded and enlarged by coupling nanofabricated devices that express memristive phenomena with biological processes, for introducing novelty and bringing new solutions to the biosensing field.

5.2   Nanofabricated Memristive Sensors for Bio-detection

Nanowire arrays are emerging as promising building blocks for miniaturized bioassays. In the case of the memristive nanowires, the biosensing is based on the variations of a voltage difference introduced in the semi-logarithmic current-to-voltage characteristics upon the introduction of charged substances on the surface. The memristive nanowires are realized by using commercially available Silicon-on-Insulator wafers and the nanofabrication can be summarized in two electron-beam (e-beam) lithography masks. The first e-beam lithography mask is dedicated to the definition of the nanodevice electrodes. The electrodes creation is realized through Nickel (Ni) evap-
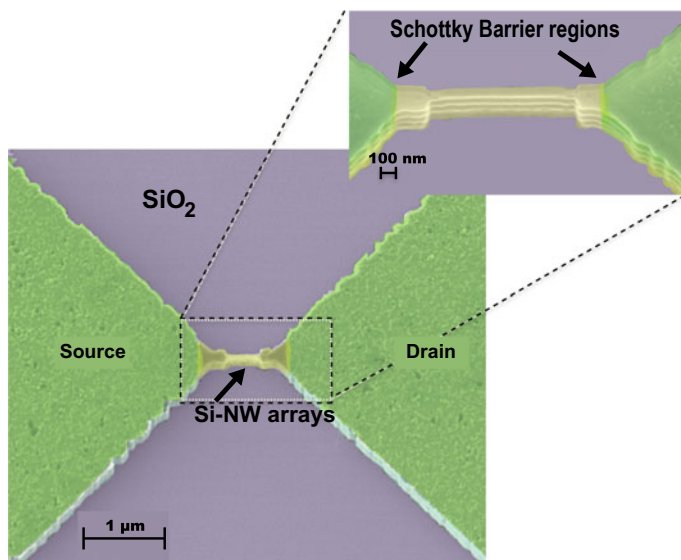
Fig. 5.1 SEM top and tilted view of the vertically stacked nanowire structures bridging NiSi source and drain contacts (Reproduced with permission from [3]. Copyright 2016 American Chemical Society)

oration, liftoff, and annealing processes. The second e-beam lithography operation is performed for the nanowire patterning, and then as a last step, the nanowire structures are etched through repeated Bosch process etching cycles of the upper Si. Overall, this process results to suspended, vertically stacked, two-terminal, Schottky-barrier Si nanowire arrays anchored between the two nickel silicide (NiSi) pillars (Fig. 5.1) for devices designed with a smaller geometry, i.e., length of 420 nm and width of 35 nm, and of larger geometry, i.e., length of 980 nm and width of 90 nm (inset Fig. 5.1). The particular electrical response of those memristive nanodevices provides a label-free ultrasensitive bio-detection method. More specifically, the electrical characterization of the nanodevices is performed with double sweeping the source-to-drain voltage (Vds) at a fixed 0 V back-gate potential. One of the distinctive features of the electrical response of these nanowires is the recorded hysteresis loop that it is characteristic of a memristive system (Fig. 5.2 top). In these nanodevices, the memory effect can be attributed to the rearrangement of the charge carriers at the nanoscale due to external perturbations [4], such as an applied voltage bias. For most bare nanowire devices, this hysteresis appears fully pinched at zero voltage. In some other cases, this hysteresis is almost pinched at very close to zero voltage values due to the impact of environmental conditions, such as the ambient humidity that introduces perturbations to the conductivity of the device, affecting in great deal the memristive signals.

Typically, a modification of the hysteresis in the memristive electrical characteristics is depicted after surface treatment of the nanodevice. The charged nature of the biological molecules brings to the nanodevice an effect similar to the one brought
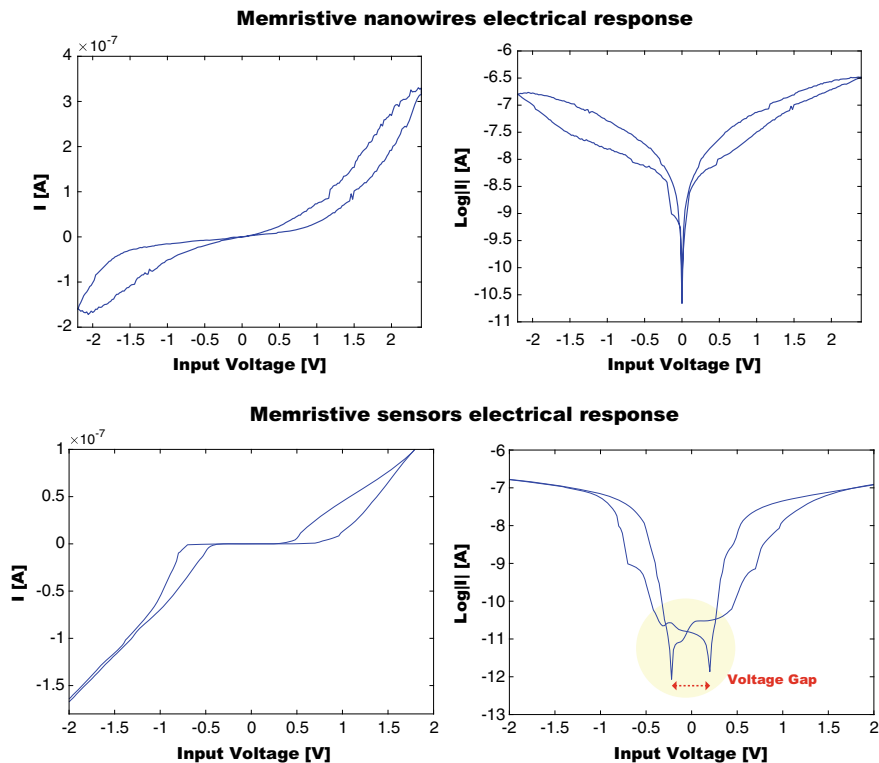
Fig. 5.2 Experimental electrical response obtained for bare two-terminal Schottky-barrier Si nanowire arrays exhibiting memristive characteristics (*memristive devices*)—top—and experimental electrical response after surface treatment (*memristive biosensors*)—bottom. The pinched hysteresis and memristive characteristics are lost giving rise to a voltage gap in the semi-logarithmic electrical characteristics

without any bio-functionalization but with the presence of an inorganic all around gate [2]. The net charge from the presence of biomolecules induces a change in the initial hysteresis creating a sort of voltage memory, appearing as a voltage difference, so-called *voltage gap*, between the current minima positions in the forward and backward branches, as a further memory effect of the voltage scan across the nanowire (Fig. 5.2 bottom) [2, 5]. More specifically, this voltage gap is dependent from the kind and the concentration of the charged substances introduced on the device surface and it is very sensitive to the charges interplay. Overall, the memristive devices are accordingly bio-functionalized with receptor molecules for obtaining *memristive biosensors* and then exposed to the target molecules providing ultrasensitive sensing through the variations of this voltage gap that consists the main bio-detection parameter.

5.2.1 Surface Treatments for Memristive Biosensors

For achieving effective and efficient bio-functionalization of the memristive nanostructures, the following main phases must be performed: *(a) Surface Activation* where hydroxylation of the surface is achieved via exposure of the surface to piranha solution (H_2SO_4–H_2O_2) or O_2 plasma, *(b) Surface pretreatment* to enable the
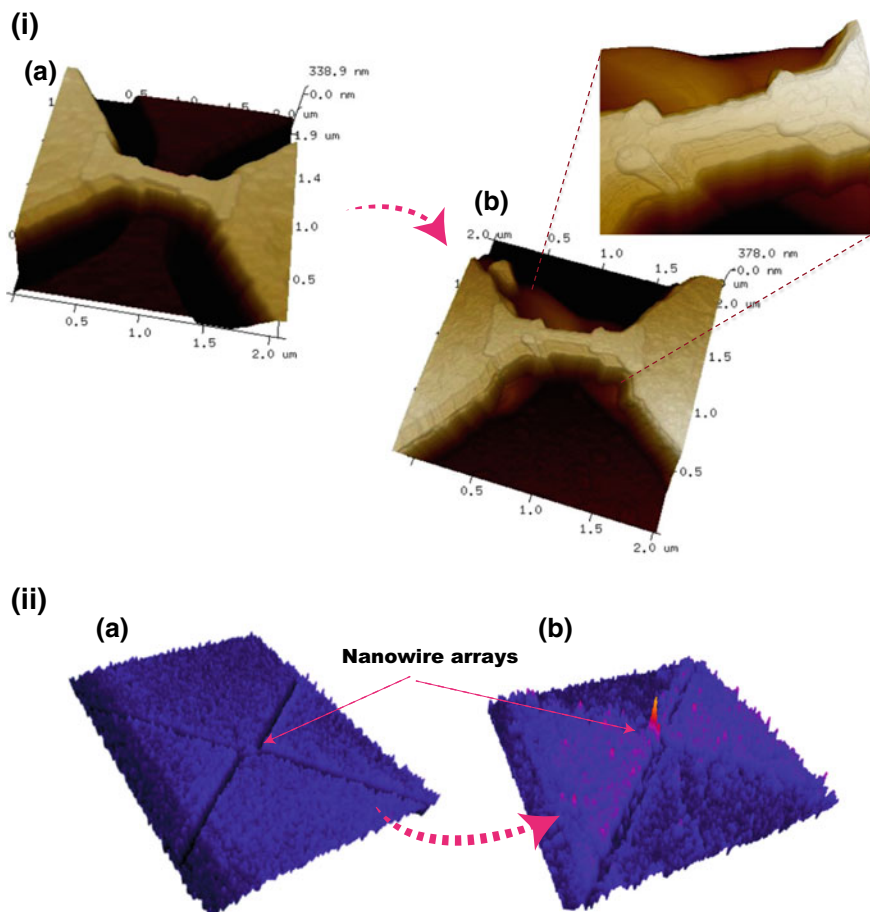

Fig. 5.3 i. AFM morphological analysis of nanowire arrays before (**a**) and after the bio-modification with an anti-Prostate Specific Antigen antibody (**b**). After bio-functionalization a clear change in the morphology can be seen and an agglomeration of biomolecules can be observed on the surface of the nanodevices masking the initial shape of the nanowires ii. Confocal microscopy of nanofabricated structures before and after bio-functionalization: 3D fluorescence signal distribution acquired using CLSM (wire-arrays of width 150 nm and length of 4.8 μm) before (control sample) (**a**) and after the bio-modification with FITC-conjugated antibodies (**b**). The bright regions in the right image correspond to the accumulated biomolecule in the sample (Reference [6]-Reproduced by permission of The Royal Society of Chemistry)

optimum receptor molecule coupling on the nanodevices' surface. These surface treatments leverage either the high affinity between biotin and streptavidin (*Affinity Approach*), or are based on covalent binding through the implementation of a silane (*Covalent Attachment*) chosen as a linker molecule or physisorption (*Direct Adsorption*) composed of interactions involving van der Waals forces, electrostatic or the much stronger hydrophobic interactions, ***(c) Receptor molecules immobilization***, namely, full-chain antibodies, antibody fragments, or DNA aptamers through adequate incubation in the receptor molecule solution. Therefore, through this step the memristive devices give rise to *memristive biosensors*, and ***(d) Exposure to target molecule*** involving disease biomarkers or/and therapeutic compounds (Fig. 5.3).

5.3 Sensing Performance of Memristive Biosensors

5.3.1 The Effect of Charged Residues—Sensing of Charged Polymeric Films[1]

The modification of the related electrical-conductivity hysteresis and the voltage gap variations due to the presence of charged macromolecules was investigated and fully characterized through the deposition of layer-by-layer charged polymeric films, i.e., via the implementation of a polyelectrolyte (PE) multilayer. PEs are linear macromolecular chains bearing a large number of charged groups when dissolved in a suitable polar solvent. Among them, PSS (Poly (sodium 4-styrene sulfonate)) is a strong polyelectrolyte negatively charged in a wide pH range while PAH (Poly(allylamine hydrochloride)) is a weak polyelectrolyte positively charged in neutral or acidic solution [7]. Subsequent depositions finally result in a PE multilayer stabilized by strong electrostatic forces [8].

The formation of PE multilayers is based on the consecutive adsorption of polyions with alternating charge using the layer-by-layer (LBL) technique as described by Chen and McCarthy [9]. The PEs multilayer is formed by consecutive alternate adsorption of positively charged PAH and negatively charged PSS prepared PE solutions. Electrical characteristics acquired (Fig. 5.4) indicated the average voltage gap value after deposition of each layer of PE for two different concentrations. The first electrical measurements were performed after -OH treatment leading to the appearance of the voltage gap. Afterward, the first PAH adsorption results in narrowing of the voltage gap (0.09 V difference for 200 nM concentration and 0.16 V difference for the case of 50 μM of PE, respectively). This change is a result of the change in the charge density at the surface of the device due to the positively charged PAH, an effect that is even more pronounced when using a higher concentration of PAH: as more positive charges are present on the surface, a larger voltage gap change is registered.

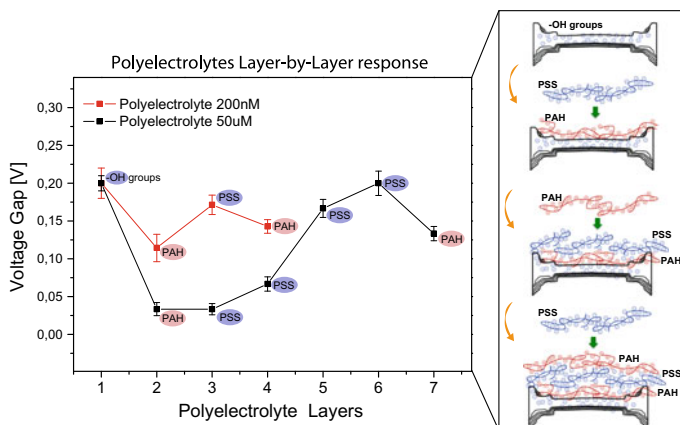---

[1] Source of original text [3].

Fig. 5.4 Formation of a multilayer of PEs by repeated electrostatic adsorption of oppositely charged PE layers; Average voltage gap value obtained from electrical characterization of devices treated with Layer-by-Layer deposition of PEs for 200 nM (red points) and 50 μM (black points) (Reproduced with permission from [3]. Copyright 2016 American Chemical Society)

The adsorption of the negatively charged PSS shifts again the average voltage gap to a higher value (0.17 V) and further treatment with PAH results in a new decrease of the average voltage gap value (0.15 V for 200 nM) concentration of PE. Therefore, it is demonstrated that further alternating exchange of the PE solution causes an alternating output signal, which slowly reduces in amplitude. On the other hand, the consecutive adsorption of the same type of PE (successive adsorption of PSS is presented in Fig. 5.4) was tested by implementing the highest concentration of PE results in the acquisition of one direction trend for the voltage gap that increases form the value of 0.05–0.21 V. Facing these interesting characteristics of the memristive nanodevices, the fabricated memristive nanostructures are thereupon applied in the biosensing field, enabling the detection of femtomolar and even attomolar concentrations. The charges interplay (positive/negative) brought by the receptor/target molecules and the concentration of the reagents (increasing/decreasing) is defining the width of the voltage gap parameter which then lands to an ultrasensitive biodetection method with an immense potential for novel biosensing.

5.3.2 Sensing Strategies

The effect demonstrated through the implementation of the charged polyelectrolytes can be correlated to the receptor/target molecule interplay. Indicatively, the effect depicted for the alternative introduction of opposite kind of charged PEs is similar to the voltage gap trend exhibited in the case of the previously reported antibody and negatively charged antigen binding (Fig. 5.5). Taking into consideration the structural composition of antibody species that consists of long amino acid chains, under

Fig. 5.5 Electrical response after bio-functionalization—black—and antigen uptake with two different biomarker concentration—blue and red—(elaborated by [2])
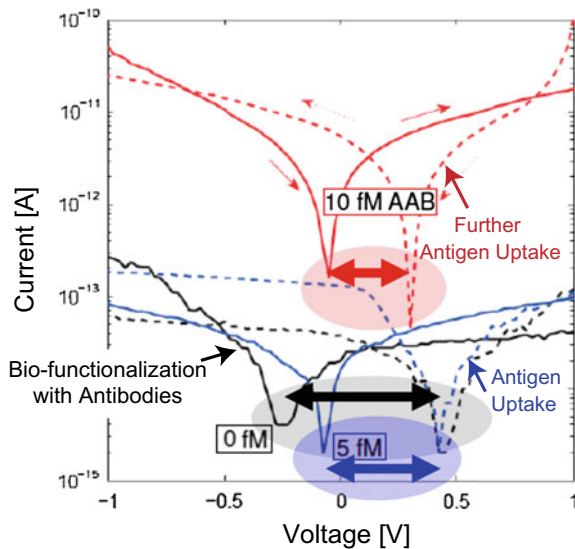
correct physiological conditions (pH 7.4) arginine and lysine residues are positively charged while aspartic and glutamic acids are negatively charged. In an antibody, positively charged residues are in excess with respect to negatively charged ones even if the charge distribution is quite similar [2]. On the contrary, antigens like PSA are negatively charged; therefore, when antibody–antigen binding occurs, an excess of negative charge accumulates at the nanowire surface that increases with respect to the increasing antigen concentration as the target molecules uptake progresses. Meanwhile, taking into consideration that aptamers are single-stranded RNA or DNA oligonucleotides, they are considered negatively charged, therefore, for aptamer and negatively charged antigen/drug pairs a one-way, increasing trend for the voltage gap is expected with the increasing antigen/drug concentration.

5.3.3 Factors Affecting the Memristive Biosensors' Performance

5.3.3.1 The In-Dry Measurement Concept

The Debye screening length between the sensor surface and the analyte determines the extent of a space charge region near a discontinuity and it is commonly introduced when performing measurements in-liquid conditions. The surface charges of biomolecules in a buffer solution are shielded by oppositely charged buffer ions in the solution, so-called *counterions*. Therefore, the Debye length may potentially mask the sensing outcomes in some cases, for instance, for extremely low sample

concentrations (Debye screening limitation). For this reason, measurements involving the *memristive biosensors* are performed not in-liquid but in-air [5], following a novel paradigm of detection via measurements in-dry conditions, under controlled relative humidity, where the sample is thoroughly dried after the exposure to the target reagent, and only an ultrathin layer of water formed by the ambient humidity is present and in high proximity to the nanowire surface. Although the sensors are dried after bio-modification and cleaning steps, the nanosensor surface is then never completely dry, allowing the proper functioning condition of the proteins and the stable and proper interactions of the probe-target molecules system [10]. Since the electrical characterization is performed in-dry conditions, there is a negligible Debye layer formation and the setup is in the framework of surface and stern layers, namely, at planes before the slipping plane. In addition, considering that the Debye length is negligible consequently, the zeta potential is negligible as well, and, therefore, the potential of interest in the suggested setup is the surface potential and its variations.

5.3.3.2 The Role of Ambient Humidity

Environmental humidity conditions on the electrical response of the nanodevice affecting to a great extent the memristive signals and the obtained hysteresis [6, 11]. The higher the humidity in the treatment area the more hydroxyl groups are introduced on to the surface of the sensor, inducing perturbations to the conductivity of the device's channel. It was observed that for low rH%, the voltage gap value for bare devices is zero or close to zero values. Increasing the rH% introduces a small voltage difference between the forward and the backward regimes, due to the presence of water molecules originating from the environmental humidity that adsorb and accumulate on the nanowire surface, finally forming a thin liquid film on the nanowire surface. The charges of water molecules act on the virtual gate voltage similarly to those of charged chemical and biological species affecting the memristive behavior of the nanodevices. It is implied that ideal pinched hysteresis, matching perfectly the theoretical aspect would be achieved by measurements performed under ideal conditions such as under high vacuum. It is worth noting that after 45% of rH%, the voltage gap is almost constant and the system appears to be saturated (Fig. 5.6). The voltage gap values in the case of bare devices are in the range of 0–0.16 V, demonstrating the stability of the device prior to any modification with respect to the humid environment.

5.3.3.3 The Size of Bio-recognition Element

An interesting relationship between the size of the bio-recognition element used and the voltage gap value measured after bio-functionalization was depicted. More specifically, the electrical performance of the biosensors was investigated in terms of the hysteresis modification for different bio-functionalization reagents, namely, full-size immunoglobulin antibodies (IgG), antibody fragments (scAb), and DNA
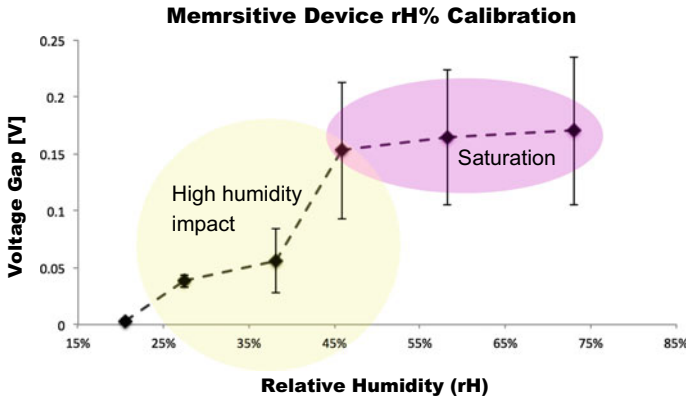
Memrsitive Device rH% Calibration

Fig. 5.6 Memristive device rH% Calibration: Average voltage gap value exhibited by non-bio-modified nanostructures just after the fabrication process tested under different relative humidity conditions (rH%)
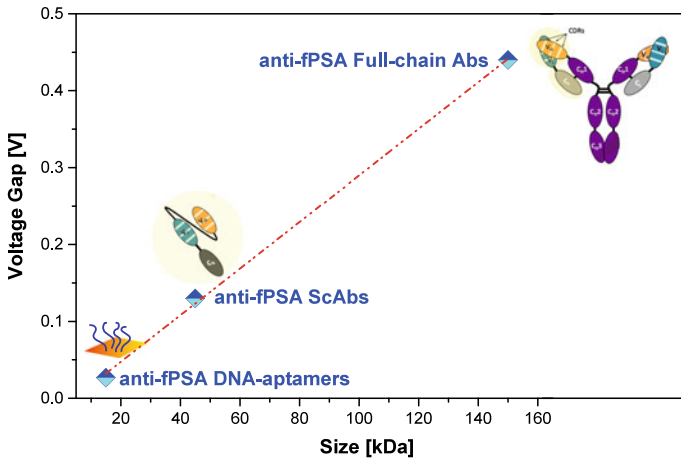

Fig. 5.7 Voltage gap dependence upon the bio-functionalization reagent: anti-PSA DNA aptamers ($\approx$15 kDa), anti-PSA ScAb ($\approx$42 kDa), and full-size anti-PSA IgG antibody ($\approx$150 kDa) demonstrate different sizes, and therefore correspond to different voltage gap values resulting in a linear trend for the voltage gap–reagent size relation [12]

aptamers. The full-size antibodies and antibody fragments implemented, demonstrate different structures and different sizes. The bio-functionalization reagents size affects the hysteresis modification, namely, the voltage gap obtained (Fig. 5.7). The voltage gap appears proportional to the antibody size that can be logically interpreted in terms of the net positive charge accumulated on the nanodevice surface and, consequently, the value of the virtual bio-gate voltage that increases with the size of the linked antibody as the net charge introduced on the nanodevice increases. A further proof to this aspect is brought by the voltage gap value of a *memristive biosensor* based

on DNA aptamers that exhibit an average molecular weight of 15 kDa. Overall, a direct relationship between the size of the bio-recognition element applied and the voltage gap value is demonstrated, showing the potential for design flexibility and compatibility with respect to the target molecules and the desired implementation, thus opening new possibilities to the fabrication of application-oriented *memristive biosensors*.

5.4 Modeling Memristive Biosensors

5.4.1 Equivalent Circuit Model Based on Memristors

Due to the wide application possibilities that memristor devices may offer, several efforts have been done to study the memristive behavior experimentally as well as computationally [13–20]. Besides theoretical aspects and experimental studies, models which approximate well the physical realization are needed. In this framework, it is worth mentioning the development of a simple compact model for representing the electrical behavior of memristors introduced by Biolek et al. [21] describing a mathematical SPICE model of the prototype of memristor, manufactured in 2008 in Hewlett-Packard (HP) Labs [13]. Furthermore, Benderli [22] suggested a macro-model which simulates the electrical behavior of the thin-film titanium dioxide (TiO_2) memristors. Last but not least in their work, Rak et al. [23] create a memristor element in Spice which simulates the published memristor realization introduced by HP Labs and offers the possibility to be used as a circuit element in design work. For the computational study of the *memristive biosensors*, a macromodel of a memristor element was created and combined with analog circuit elements forming equivalent circuit models that reproduced and emulated successfully the behavior of the physical system fitting in good approximation the experimental results of *memristive biosensors* [24]. Throughout simulations and adequate fitting between the experimental and computational outcomes, it was found that the electrical characteristics obtained from experimental measurements exhibit hysteretic properties imputable to memristive devices validating the hypothesis that the experimental setup deals with memristive behavior and confirming the memristive nature of the physical system. In addition, the voltage gap appearing at the current-to-voltage characteristics for nanowires with bio-modified surface was successfully reproduced computationally and was related to capacitive effects due to minority carriers in the nanowire [24]. It was also indicated that those effects are strongly affected by the concentration of biomolecules uptaken on the device surface.

5.4.2 Bare Si Nanowire Devices: Memristive Devices

According to previous works mentioned in literature [25–28], Si nanowire FETs with Schottky source and drain contacts can be modeled as metal–semiconductor–metal
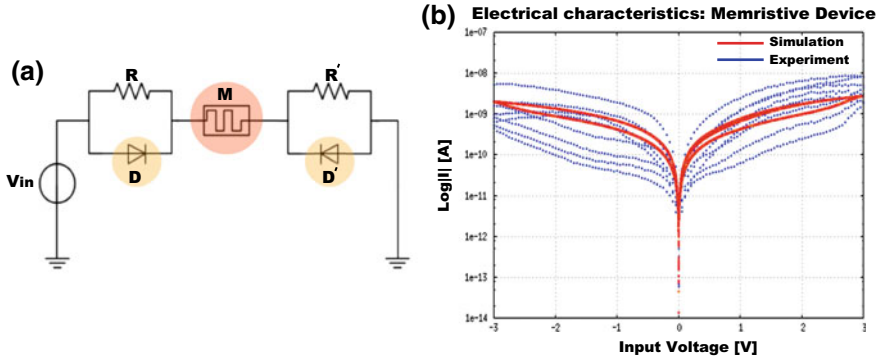
Fig. 5.8 Equivalent circuit of a memristor sandwiched between two non-identical head-to-head Schottky barriers. The sub-circuits consisting of a diode in parallel to a resistor emulate the effect of the Schottky barriers. The circuit consists of resistances in the range of 0.5 kΩ–1kΩ and common Si epitaxial planar fast switching diodes provided by SPICE (**a**). Semi-logarithmic current-to-voltage results obtained from the equivalent circuit comparing to experimental results coming from electrical measurements of bare memristive device (**b**). The simulation current is scaled accordingly to the experimental current range and the input voltage amplitude is [−3:3] Volts. Since, by nature the devices usually present a non-identical behavior multiple experimental curves are presented and it is demonstrated that the computationally obtained results follow in good approximation the average behavior of the physical system, and it can be concluded that the experimental setup exhibits memristive behavior (elaborated by [24])

(M-S-M) structures with finite Schottky-barrier heights. The modeling is based on equivalent circuits including a Schottky diode representing the metal–semiconductor contacts and considering the nanowire as a resistor. Lee et al. [27] developed an equivalent circuit model which consisted of one reverse-biased Schottky diode, one resistor, and one forward-biased Schottky diode connected in series. Thus, the intrinsic nanowire channel is modeled as one linear resistor and the gate voltage dependence of the nanowire was not included. In addition, there has also been introduced [25] a Si nanowire FET model based on an equivalent circuit consisting of two Schottky diodes for the M-S contacts and one MOSFET for the intrinsic Si nanowire FET. Furthermore, Elhadidy et al. [26] modeled the symmetrical, nonlinear current-to-voltage characteristics of a metal–semiconductor–metal structure of two metallic Schottky contacts fabricated to a p-type semiconductor by treating the semiconductor as a resistor sandwiched between two identical head-to-head Schottky barriers. Each one of the two Schottky barriers is modeled as a sub-circuit consisting of a diode in parallel to a resistor (Fig. 5.8). For the case of the memristive nanowires, an equivalent circuit model was developed by following the concept introduced by Elhadidy et al. [26] consisting of a memristor sandwiched between two identical head-to-head Schottky barriers [24]. The Schottky barriers were represented by (RD) sub-circuits consisting of a diode in parallel to a resistor and result in a slight modification of the memristive curve, bringing the typical Schottky contact shape at the branches, without affecting the location of the current minima. A unique current corresponds to each applied voltage. If the polarity of the bias voltage is exchanged, the reverse-biased barrier

would be exchanged with the forward-biased one and vice versa. For consistency reasons and interest, the input values of the sinusoidal Voltage (Vin) source were the same with respect to the case of the pure memristor equivalent circuit. Experimental current-to-voltage characteristics present noticeable asymmetry at the branches of the semi-logarithmic current-to-voltage characteristics. Under ideal circumstances, the electrical characteristics in both branches of the semi-logarithmic current-to-voltage curve would be symmetrical since the Schottky barriers of the device structure are considered to be identical. Nevertheless, the measured data in real experimental conditions indicates non-identical branches for the majority of the devices under study. This slight difference in the branches asymmetry may be explained as a consequence of the non-identical area of contacts occurring in the real conditions, mainly due to the presence of the different interfacial insulating layers at both electrode contacts. In order to emulate this asymmetry arising in the physical system, and considering that the one diode does not conduct during the one circle of the voltage, as mentioned before, the equivalent circuit in this specific case could be simplified by replacing the one of the two autonomous sub-circuits (RD) by a resistor. Therefore, the concept of the non-identical Schottky barriers is taken into consideration in the equivalent electrical circuit through the equivalent resistor, and in combination to the fact that during the one circle of the current (depending on the polarity of the bias voltage) the one diode does not conduct due to the forward and reverse bias nature of the diode and consequently only the remaining resistivity origin from the reverse-biased Schottky diode finally contributes. It was demonstrated that the simulation results followed in good approximation the average behavior of the physical system, and presented current-to-voltage characteristic curve equivalent to that of a memristor device electrically contacted by two asymmetric Schottky barriers, validating the hypothesis that the experimental setup deals with memristive behavior.

5.4.3 Bio-functionalized Silicon Nanowire Devices: Memristive Biosensor

A Schottky diode can also be described with an equivalent circuit model consisting of a nonlinear capacitor in parallel to a nonlinear resistor according to literature [29]. The capacitor stands for the space charge capacitance and reflects only the free carriers of the material, while the resistor represents the residual conductance of the diode. In the case of lightly doped materials, the free-carrier concentration can become comparable to the deep level concentration, and in this case, charged and recharged deep levels also contribute considerably to the measured capacitance. In a Schottky barrier, the barrier is high enough that there is a depletion region in the semiconductor near the interface. In the depletion region of the Schottky barrier, dopants remain ionized and give rise to the "space charge" which, in turn, gives rise to a capacitance of the junction. The metal–semiconductor interface and the opposite boundary of the depleted area act like two capacitor plates, with the depletion region acting as a dielectric. The amount of junction capacitance initially depends on the applied terminal voltages. By applying a voltage to the junction, the width of the
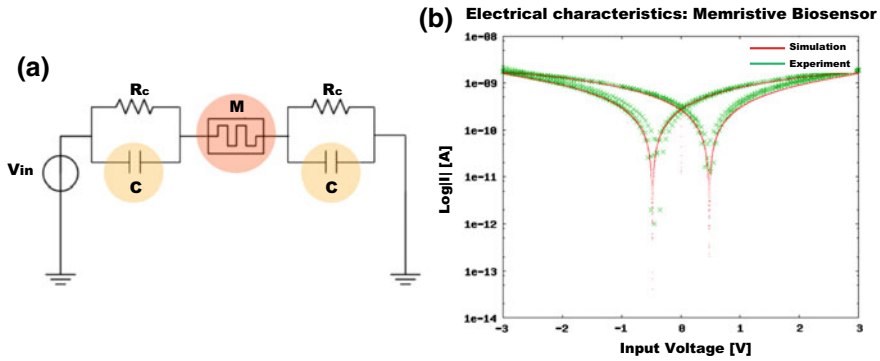
(a)

(b) Electrical characteristics: Memristive Biosensor

Fig. 5.9 Equivalent circuit for *memristive biosensors* consisting of a memristor and nonlinear sub-circuits (RC). The sub-circuits (RC) introduced consist of a nonlinear capacitor in parallel to a nonlinear resistor (**a**) and semi-logarithmic current-to-voltage results simulation (red curve) obtained from the equivalent circuit, as compared to experimental results coming from electrical measurements for the case of *memristive biosensor*, namely, the nanofabricated device after the bio-functionalization with antibodies, for three voltage sweeps (green curves). The simulation current is scaled accordingly to the experimental current range. The input voltage amplitude is [−3:3] Volts and the resistances value at 0.85 kΩ (elaborated by [24])

space charge layer will be shifted and the space charge within the depletion region will vary, since additional defect centers will be ionized, and as a result the capacitance will also be different. Furthermore, the charging and recharging of the trap levels during a measurement cycle periodically change the Schottky-barrier height, and finally the modified measurement current gives a capacitive contribution to the diode admittance. Thus, both effects, variation of bias and consequently the ionization of traps, cause a change in the junction capacitance [30]. An equivalent circuit containing nonlinear sub-circuits (RC) consisting of a nonlinear capacitor in parallel to a nonlinear resistor was further then introduced (Fig. 5.9a) in order to correctly model the appearance of the voltage gap, for the case of *memristive biosensors*. The sub-circuits were connected in series to the memristor (M) of the initial equivalent circuit. It was demonstrated (Fig. 5.9b) that the two current minima are clearly separated and a voltage gap appears in the semi-logarithmic current-to-voltage characteristics due to the presence of the capacitors now introduced. The fitting of the simulation results with the experimental data confirms that the voltage gap appearing at the experimental current-to-voltage characteristics for the *memristive biosensors* was computationally reproduced successfully and fitted in very good approximation with the experimental outcomes. Measurement of the junction capacitance is a very useful technique, giving information on Schottky-barrier heights, dopant profiles, as well as the presence of traps and defects inside the semiconductor and at the interface [31]. Accumulating evidence from several works concerning relevant measurements [29–32] report values for capacitances that appear in the junction area that refers to the space charge capacitance, to belong in the range beginning of pF [29, 30] and reaching the values of nF [31, 32]. According to literature, the excess capacitance

is a result of the combination in parallel of the space charge capacitance characterizing the diode and of the diffusion capacitances due to the injection of minority carriers. The reported values concerning the excess capacitance reach 43 nF and it is considered that the excess capacitance mainly originates from the bulk Si rather than the interface of the diode in study [32] while typical capacitance values concerning only contributions by the depletion area are in the range of pF [29, 30]. It is worth mentioning that all the values found for the equivalent capacitance fit quite well the values reported in literature concerning the excess capacitance, and thus it is demonstrated that the presence of antibodies and thereafter of antigens on the *memristive biosensor* interacts deeply with the conductivity of the channel related to minority carriers. The width of the simulated voltage gap can be modulated by the variation of the value of the capacitance introduced in the circuit. More specifically, it is observed that the two local minima are converging or shifting away the one from the other by modifying the input values of the capacitance introduced to the equivalent circuit. Experimental observations [2] identify a similar behavior of voltage gap modification with respect to the type and the concentration of the biological molecules uptaken on the device surface, and an enlargement of the hysteresis window due to the presence of charged molecules around the freestanding channel, i.e., the antibodies, after the bio-functionalization process, are experimentally noticed. Accumulating data suggests that the maximum voltage gap observed is of a value of 1 V approximately.

5.4.4 Antigen Uptake

The presence of antigens on the device surface seems to demonstrate the opposite effects comparing to those resulting due to the presence of the antibodies. Antigens are considered to have a masking contribution to the presence of antibodies all around the device and decrease the positive charge effect due to the presence of antibodies after the bio-functionalization process. Thus, the uptake of antigens acts by decreasing the value of the positive all around gate bias voltage created by the presence of antibodies. According to the previous arguments, the presence of antigens also affects

Table 5.1 Voltage gap values obtained experimentally for different antigen concentrations and computationally estimated voltage gap values for different values of capacitance, selected according to the experimental data. For 0 fM concentration of antigens, it is considered that the voltage gap that appears is created only due to the bio-functionalization with antibodies

Antigen concentration (fM)	Voltage gap (V) *-experimental-* [2]	Capacitance (nF)	Voltage gap (V) *-simulation-*
0	0.84	36	0.844
5	0.56	24	0.563
10	0.37	15	0.362

the width of the voltage gap, which is already created by the presence of antibodies all around the device after bio-functionalization. Collectively, the experimental data depicts a contraction of the hysteresis window with increasing the concentration of antigens. To further define the role of the capacitance value to the voltage gap, the experimentally obtained results concerning voltage gap values for different antigen concentrations [2] were taken into consideration and different capacitance values were introduced to the aforementioned equivalent circuit (Fig. 5.9a) designed for simulating the modified-memristive behavior, in order to reproduce computationally the voltage gap values obtained experimentally as reported in Table 5.1. Furthermore, the calibration curve (Fig. 5.10) depicted the computationally estimated voltage gap values that equal the values of the voltage gap obtained experimentally [2] for different antigen concentrations. The computationally obtained voltage gap values are a result of the different equivalent capacitance values introduced to the equivalent circuit and it is found that corresponds to the values reported in literature for the excess capacitance [32]. Intermediate theoretical values for the voltage gap obtained from simulations for different capacitance values are also shown in the figure (Fig. 5.10). It can be noticed that for achieving narrower voltage gaps lower values for the capacitance must be introduced to the equivalent circuit for reproducing computationally the corresponding experimental obtained voltage gap. This evidence suggest that
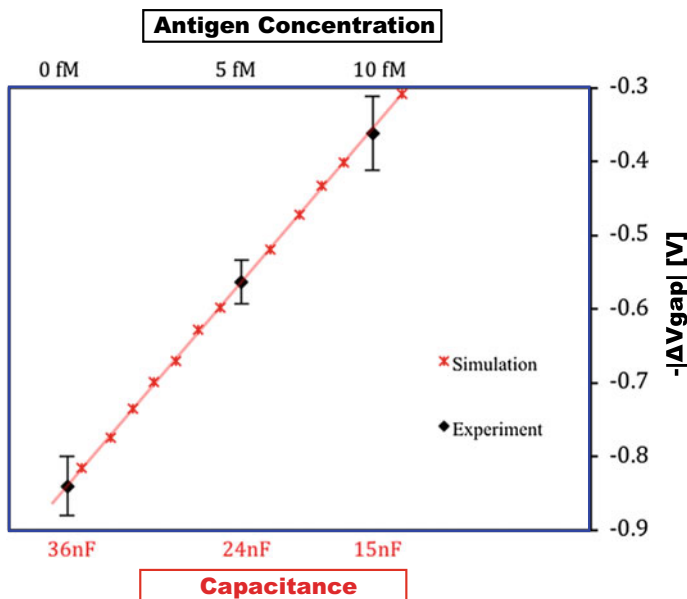

Fig. 5.10 Calibration curve obtained experimentally for three concentrations. The uptake with antigens modifies the memristive behavior such as -|Vgap| increases with the increase of the antigen concentration. For 0 fM concentration of antigens, it is considered that the voltage gap that appears is created only due to the bio-functionalization with antibodies. The theoretical values for the voltage gap are results obtained from simulations for different capacitance values (elaborated by [24])

increasing the concentration of antigens demands lower values for the capacitance introduced to the equivalent circuit in order to achieve the same value for the voltage gap, with respect to this range of capacitance values. For zero concentration of antigens (0 fM), only the voltage gap already created by the presence of antibodies after the bio-functionalization process is considered.

5.5 Memristive Aptasensors

Aptamers are synthetic,[2] single-stranded RNA or DNA oligonucleotides 15–60 base in length. These nucleic acid ligands have small molecular weights (ranging from 5 to 15 kDa) and are chemically developed to bind with high specificity and selectivity to a specific target analyte, like, for example, a protein, by undergoing a conformational change. More specifically, the interaction of aptamers with the target is based on the 3D folding patterns. The complex 3D structure of the single-stranded oligonucleotide is due to the intramolecular hybridization, which causes the folding into particular shape. Aptamers fold into tertiary conformations and bind to their targets through shape complementarity at the aptamer–target interface [34].

DNA aptamer, along with antibodies, is very suitable candidates for the design of novel and highly specific biosensors. Moreover, DNA aptamers exhibit many advantages such as the possibility for supporting continuous monitoring, enhanced stability, specificity, and reproducibility. Moreover, the well-established synthesis protocol and chemical modification technology is a key benefit that encloses the use of aptamers, leading to rapid, large-scale synthesis and modification capacity that includes a variety of functional moieties, low structural variation during chemical synthesis, and lower production costs. Aptamers can bind to nucleic acid, proteins, small organic compounds, phospholipids, iron channels, and even whole cells [35, 36].

5.5.1 Memristive Aptasensors for Diagnostics

DNA-aptamer-based *memristive biosensors* so-called as *memristive aptasensors* (biotinylated anti-PSA DNA aptamer solution (5ʹ-[biotin tag] TTT TTA ATT AAA GCT CGC CAT CAA ATA GCT TT-3ʹ) were investigated for their analytical performance at biomarker sensing for prostate cancer as a case of study. The PSA (PSA, 30 kDa Kallikrein protein) at different concentrations in the range of [aM-pM] was then used as a model of target diagnostic molecules. Electrical characterization performed indicated voltage gap openings after the bio-modification of the device with DNA aptamers and increasing antigen concentration (Fig. 5.11a, b). An increasing one-way trend for the voltage gap was recorded reaching saturation at some tens

---
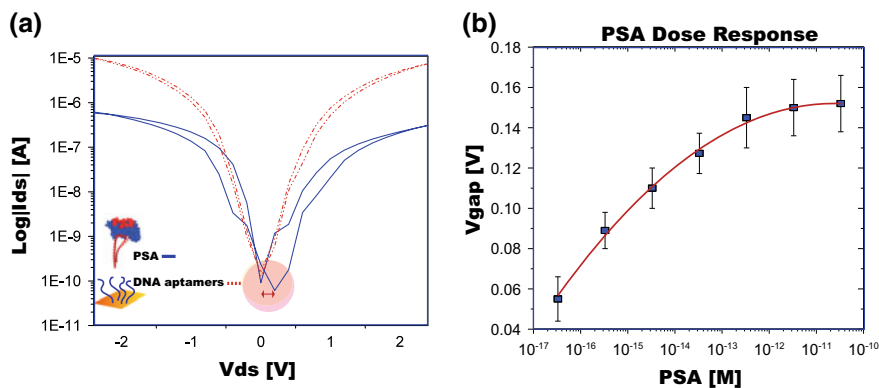
[2]Source of original text [3, 33].

Fig. 5.11 Representative electrical characteristics and PSA dose response of memristive aptasensor: Indicative electrical characteristics demonstrating the introduction of the voltage gap occurring upon bio-modification of the surface of the nanodevice (**a**). Calibration curve related to the average voltage gap versus dose response (**b**) (Reproduced with permission from [3]. Copyright 2016 American Chemical Society)

Table 5.2 State-of-the-art list of reported PSA electrochemical aptasensors to date

Method	Electrode surface	LOD	References
SWV	GCE	pM range	[37]
EIS	Gold electrodes	30 pM	[38]
DPV	GCE	7.6 pM	[39]
EIS	GCE	0.15 pM	[40]
EIS	Gold electrodes	fM range	[41]
EIS(capacitance measurements)	Gold electrodes	30 fM	[42]
DPV	GCE	300 aM	[40]
Memristive aptasensor	Si-nanowires	23 aM	[3]

SWV square wave voltammetry, *EIS* electrochemical impedance spectroscopy, *DPV* differential pulse voltammetry, *GCE* glassy carbon electrode

of pM. This outcome signifies that we are within and actually slightly below the clinical range (critical level of PSA 4 ng/mL ca. 133 pM). This fact allows working with highly diluted samples, significantly low volumes of clinical samples from the patient are required and the detection at early stages can be achieved. An extremely ultralow LOD of 23 aM was achieved thank to the implementation of the *memristive aptasensors*. The LOD achieved was the best ever obtained among electrochemical biosensors for PSA so far reported in literature (Table 5.2).

Furthermore, the nanofabricated structures are exposed to PSA prepared in non-diluted, full human serum considering concentrations below the clinical range, offering a proof of the capability of the sensor to function in extremely low concentrations of biomarkers and the acquisition of the increasing trend resulted by the introduction of the increasing negative charge on the surface of the nanodevice.

5.5.2 Memristive Aptasensors for Therapeutics

Having demonstrated the direct and highly efficient response of the nanobiosensor prototype to accurately follow the various steps of DNA aptamer binding-regeneration cycle, the memristive properties of the nanosensors are further leveraged for the label-free, ultrasensitive detection of therapeutics compounds (drugs), bringing a completely new perspective for the label-free monitoring personalized and precise medicine. Ultrasensitive drug screening is a key aspect in the field of therapeutics. As therapeutic compounds are going to be supplied in less and less concentration, the need for more sensitive detectors presents immense importance. Therefore, *memristive aptasensors* resulting in ultrasensitive sensing outputs with cancer biomarkers were implemented for effective ultrasensitive drug screening as well. The implementation of DNA aptamers also offers the potential for the nanosensor regeneration, opening the way for continuous monitoring of therapeutic compounds, a very significant requirement in therapeutics. To better show the performance of the proposed new biosensors, Tenofovir (TFV), an antiviral drug for HIV treatment, is considered here as a model drug. The therapeutic range concentration of TFV in the circulatory plasma of some nM up to 860 nM. TFV-aptamers (5'-Aptamer-C6 Amino-3') developed for specific interaction with TFV were immobilized on the surface of the memristive devices and the detection was performed for drug concentrations belonging within and slightly below the clinical range, opening to the possibility for future applications with minimum requirements of amount of clinical samples (Fig. 5.12).
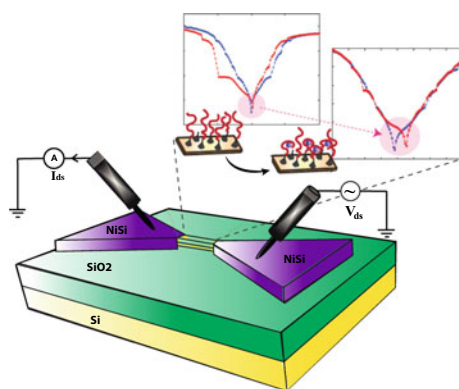

Fig. 5.12 Schematic representation illustrating the memristive sensor, and SEM micrograph depicting the Si-NW arrays anchored between the NiSi pads, which serve as electrical contacts of the freestanding memristive nanodevice. The position of the current minima for the forward and the backward regimes changes after the surface treatment introducing a voltage difference in the semilogarithmic current-to-voltage characteristics (Reference [33]-Reproduced by permission of The Royal Society of Chemistry)
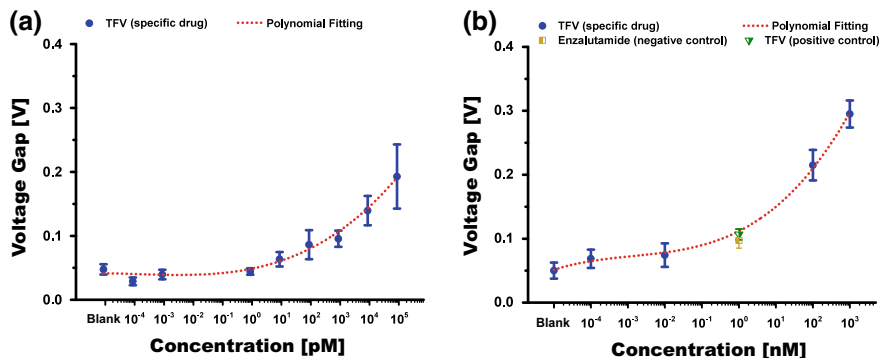
Fig. 5.13 Analytical performance and effective drug detection through the electrical hysteresis variations in buffer (**a**) and in full human serum (**b**). For the in serum detection, a new drug detection is performed following regeneration of the *memristive aptasensor*. The response of the sensor to the new drug binding fits ideally the calibration curve obtained initially. The exposure of the sensor directly after, to a nonspecific drug, does not result in any signal difference (Reference [33]-Reproduced by permission of The Royal Society of Chemistry)

The successive uptakes of negative charge at the nanodevice surface led to an increasing trend of the voltage gap following the increasing concentration of the detection target drug. An increasing trend of this parameter of the hysteresis is then depicted following the dose increase (Fig. 5.13a) till the value of 193 ± 51 mV for 100 nM, the highest concentration implemented for the case of buffer solution. In human serum, a hysteresis modification (69 ± 38 mV) is initially indicated for a concentration of 100 fM and reaches finally the value 295 ± 61 mV for 1 μM (Fig. 5.13b). At the end of the dose-response cycle in the human serum, a regeneration step was performed and an intermediate TFV concentration of 1 nM was applied. It was depicted that indeed the signal obtained for the hysteresis voltage gap (97 ± 31 mV) was back to the value foreseen by the previously recorded dose-response curve. This results clearly demonstrate the efficiency and consistency of the proposed method, and its applicability for continuous monitoring of therapeutic compounds as well. Furthermore, the implementation of a negative control drug, enzalutamide (a widely used anti-prostate cancer drug) was performed as an additional step. Indicatively, the voltage gap (89 ± 35 mV) obtained for the negative control brought no significant hysteresis modification (<9% difference) for the very same drug concentration of 1 nM, thus no drug binding occurred for the negative control case, exhibiting the extremely good specificity of the methodology applied. A very low LOD of 3.09 pM for PBS buffer and of 1.38 nM for human serum was demonstrated achieving optimum performance comparing to the so far reported state of the art for drug detection, in general, and for TFV in particular (Table 5.3). These LODs demonstrated 10 times better performance for the in buffer drug detection with respect to the literature and show twice better performance for drug sensing in human serum, ever obtained.

Table 5.3 State-of-the-art list of reported drug detection to date

Target drug	Method	Surface	LOD (nM) Buffer/bio-matrix	Linear Range (nM)	References
ART	Ampero	GrPnano	0.031/ 0.035[+]	0.13–1	[43]
CLE	Voltam	BZ GNPs	–/43.96[•]	100–800	[44]
CAM	Ampero	Cds-NPs/GNPs	0.14/–	0.15–2.94	[45]
Gleevec	Conduc	Si-NW	–/–	Up to 100	[46]
6-MP	Voltam	GRA/Ppy/MWCNTs	–/80*	200–100000	[47]
PCM	Voltam	MWCNTs	2.9/–	5–1000	[48]
PCN	Voltam	B-diam	–/320**	400–100000	[49]
TAM	Voltam	Enz/PN/Pt	0.2/–	27–297	[50]
TFV	BSI	Glass chip	2.5/–	Up to 20	[51]
TFV	LC-MS	–	–/680[++]	1360–350000	[52]
TFV	Voltam	HMDE	450/870[⋆]	Up to 17000	[53]
TFV	LC-UV	–	–/10.4	35–3480	[54]
TFV	LC-MS	–	–/7	35–3480	[54]
TFV	Memristive	NW arrays	0.0031/1.38[⋆⋆]	0.001–1000	[33]

ART artesunate, *CLE* clenbuterol, *CAM* chloramphenicol, *PCM* paracetamol, *PCN* penicillin, *TAM* tamoxifen, *6-MP* 6-mercaptopurine, *Voltam* voltammetry, *Conduc* conductance, *Ampero* amperometry, *BSI* back scattering interferometry, *LC* liquid chromatography, *MS* mass spectroscopy, *UV* ultra violet, *GrPnano* Gr-polyaniline nanocomposite, *BZ GNPs* benzedithiol-gold nanoparticles, *GRA/Ppy* graphite/polypyrrole, *B-diam* boron-dopped diamond, *Enz/PN* enzyme/polyaniline
*Diluted human urine sample; **Human urine sample; [•]Diluted rat urine sample; [+] Highly diluted human serum; [++]Human urine; [⋆]Diluted/precipitated human plasma; [⋆⋆]Full human serum

5.5.3 Aptamer Regeneration Through the Perspective of Memristive Phenomena

The regeneration properties of the DNA aptamers were directly reflected on the *memristive aptasensors* response as expressed through a voltage difference appearing in the semi-logarithmic current-to-voltage characteristics. The whole sensing cycle consisting of aptamers immobilization, target-drug binding, aptamer regeneration, and target-drug rebinding was for first time portrayed through the variations of the electrical hysteresis of the memristive nanostructures. A series of denaturation, pH shocking, and refolding is used for surface regeneration (unbound the target from aptamer and restore the aptamers to their previous folded and functional form). After treatment with DNA aptamers, the electrical response of the nanodevices indicated a voltage difference of 116 ± 34 mV. Following the nanodevices exposure to the negatively charged target drug solution of 100 nM, an increase of the voltage difference occurs as an aftereffect of the drug binding, reaching the value of 156 ± 24 mV (increase of 34.5%). However, the most promising outcome undoubtedly lays on the electrical response after the regeneration of aptamers that follows the drug binding. It was demonstrated that the voltage difference was decreased after the regeneration process back to the blank level (to the value of 120 ± 15 mV), namely, at the level that corresponds to the value obtained initially just after the aptamer immobilization on the surface. In order to verify the reliability of the nanobiosensor in repeated measures and the capability for further capturing and detecting the target molecules after

the aptamers regeneration, and the biosensors response to a different concentration of the sensing target, the very same nanodevices were anew exposed to the drug solution but this time, a higher concentration of $1\,\mu M$ is introduced. A higher concentration of reagent implies higher negative charge density and, as expected, the uptake of higher concentration of the drug resulted in a more pronounced modification of the voltage gap. In this case, a 100% increased signal was acquired and the voltage difference indicates the value of $240 \pm 23\,mV$ that was twice the signal exhibited by DNA aptamers. It is worth to mention that the percentage of the signal difference for the hysteresis modification between the two different drug concentrations is estimated around 53.8%. Finally, a further regeneration step was carried out to illustrate the nanobiosensors repeated regeneration character. It is indeed demonstrated that the voltage difference $(121 \pm 39\,mV)$ registered after this further regeneration process coincided with the value achieved initially for the aptamer immobilization on the surface that was also the same to the one obtained after the first regeneration. That means the biosensors is very reproducibly down to the original value of the voltage gap after any regeneration process and, therefore, ready for a new measure of the target molecule concentration. The reproducibility of the device presented as the percentage differences between the hysteresis modification signals obtained after the initial aptamer immobilization and the two regeneration procedures applied is around 3.4% and 4.3% for these two regenerations, respectively. Those percentages can be considered negligible indeed, since these differences are approximately five times less the values of measurement errors usually obtained in detection on drug binding. Overall, it is worth highlighting that all these findings indicate a clear evidence that DNA aptamer natural characteristics to binding to drugs and related functions may indeed be efficiently transduced by using the memristive phenomena (Fig. 5.14).
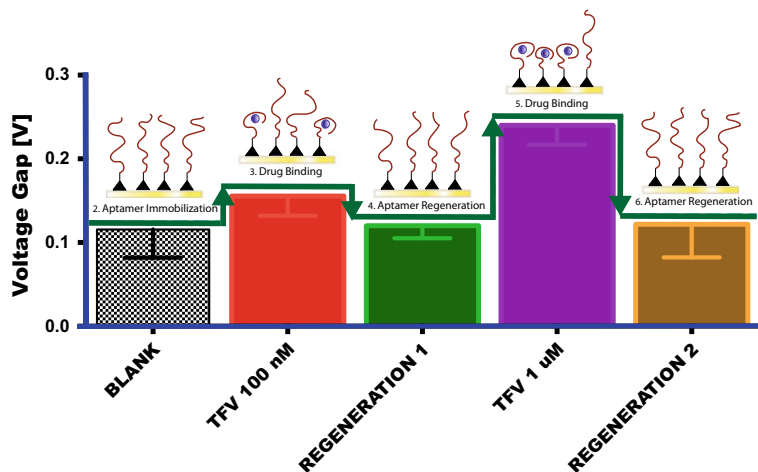

Fig. 5.14 DNA aptamer immobilization, target molecule binding, and DNA aptamer regeneration cycle, illustrated through the electrical hysteresis variations (Reference [33]-Reproduced by permission of The Royal Society of Chemistry)

5.6 Conclusions

As we have seen in this chapter, the coupling of memristive effect with biological processes gives us innovative nanobiosensing new technologies with un-precedent high performance in both diagnostics and therapeutics. Silicon nanowire arrays exhibiting a memristive effect and sophisticated bio-functionalization give rise to now kind of biological sensors: the *Memristive Biosensors*. This completely new class of biosensors successfully addresses the issues of an early detection of cancer since it provides high performance, ultrasensitive, label-free electrochemical sensing of extremely small traces of cancer biomarkers, such as the PSA, as well as effective screening and continuous monitoring of therapeutic compounds, such as TFV, also in full human undiluted serum. This powerful capability of such a new approach opens to new solutions in the medical practice, especially in the field of personalized and precision medicine.

References

1. M.-A. Doucey, S. Carrara, Nanowire sensors in cancer. Trends Biotechnol. (2018)
2. S. Carrara, D. Sacchetto, M.-A. Doucey, C. Baj-Rossi, G.D. Micheli, Y. Leblebici, Memristive-biosensors: a new detection method by using nanofabricated memristors. Sens. Actuators B Chem. **171–172**, 449–457 (2012)
3. I. Tzouvadaki, P. Jolly, X. Lu, S. Ingebrandt, G. de Micheli, P. Estrela, S. Carrara, Label-free ultrasensitive memristive aptasensor. Nano Lett. **16**(7), 4472–4476 (2016)
4. Y.V. Pershin, M. Di Ventra, Memory effects in complex materials and nanoscale systems. Adv. Phys. **60**(4), 145–227 (2011)
5. F. Puppo, M. Di Ventra, G. De Micheli, S. Carrara, Memristive sensors for ph measure in dry conditions. Surf. Sci. **624**, 76–79 (2014)
6. I. Tzouvadaki, N. Madaboosi, I. Taurino, V. Chu, J.P. Conde, G. de Micheli, S. Carrara, Study on the bio-functionalization of memristive nanowires for optimum memristive biosensors. J. Mater. Chem. B **4**(12), 2153–2162 (2016)
7. T. Mauser, C. Déjugnat, G.B. Sukhorukov, Reversible ph-dependent properties of multilayer microcapsules made of weak polyelectrolytes. Macromol. Rapid Commun. **25**(20), 1781–1785 (2004)
8. H. Riegler, F. Essler, Polyelectrolytes. 2. intrinsic or extrinsic charge compensation? Quantitative charge analysis of pah/pss multilayers. Langmuir **18**(8), 6694–6698 (2002)
9. W. Chen, T.J. McCarthy, Layer-by-layer deposition: a tool for polymer surface modification. Macromolecules **30**(1), 78–86 (1997)
10. F. Puppo, M. Doucey, J. Delaloye, T.S.Y. Moh, G. Pandraud, P.M. Sarro, G.D. Micheli, S. Carrara, Sinw-fet in-air biosensors for high sensitive and specific detection in breast tumor extract. IEEE Sens. J. **16**(10), 3374–3381 (2016)
11. F. Puppo, A. Dave, M. Doucey, D. Sacchetto, C. Baj-Rossi, Y. Leblebici, G.D. Micheli, S. Carrara, Memristive biosensors under varying humidity conditions. IEEE Trans. NanoBioscience **13**(1), 19–30 (2014)
12. I. Tzouvadaki, J. Zapatero-Rodriguez, S. Naus, G. de Micheli, R. O'Kennedy, S. Carrara, Memristive biosensors based on full-size antibodies and antibody fragments. Submitted to Sens. Actuator B-Chem
13. D.B. Strukov, G.S. Snider, D.R. Stewart, R.S. Williams, The missing memristor found. Nature **453**(5), 80–83 (2008)

14. M.D. Ventra, Y.V. Pershin, L.O. Chua, Circuit elements with memory: memristors, memcapacitors, and meminductors. Proc. IEEE **97**(10), 1717–1724 (2009)
15. A. Gelencsér, T. Prodromakis, C. Toumazou, T. Roska, Biomimetic model of the outer plexiform layer by incorporating memristive devices. Phys. Rev. E **85**(4), 041918 (2012)
16. J.J. Yang, M.D. Pickett, X. Li, D.A. Ohlberg, D.R. Stewart, R.S. Williams, Memristive switching mechanism for metal/oxide/metal nanodevices. Nat. Nanotechnol. **3**(7), 429–433 (2008)
17. S. Shin, K. Kim, S.M. Kang, Compact models for memristors based on charge-flux constitutive relationships. IEEE Trans. Comput. Aided Des. Integr. Circuits Syst. **29**(4), 590–598 (2010)
18. D. Biolek, M. Di Ventra, Y.V. Pershin, Reliable spice simulations of memristors, memcapacitors and meminductors. Radioengineering **22** (2013)
19. I. Vourkas, A. Batsos, G.C. Sirakoulis, Spice modeling of nonlinear memristive behavior. Inter. J. Circuit Theory Appl. **43**(5), 553–565 (2015). CTA-13-0128
20. F. Puppo, F.L. Traversa, M.D. Ventra, G.D. Micheli, S. Carrara, Surface trap mediated electronic transport in biofunctionalized silicon nanowires. Nanotechnology **27**(34), 345503 (2016)
21. Z. Biolek, D. Biolek, V. Biolkova, Spice model of memristor with nonlinear dopant drift. Radioengineering **18**(2), 210–214 (2009)
22. S. Benderli, T.A. Wey, On spice macromodelling of tio2 memristors. Electron. Lett. **45**(7), 377–379 (2009)
23. A. Rak, C. Gyorgy, Macromodeling of the memristor in spice. Trans. Comp. Aided Des. Integ. Circuit Sys. **29**, 632–636 (2010)
24. I. Tzouvadaki, F. Puppo, M. Doucey, G.D. Micheli, S. Carrara, Computational study on the electrical behavior of silicon nanowire memristive biosensors. IEEE Sens. J. **15**(11), 6208–6217 (2015)
25. S.H. Lee, Y.S. Yu, S.W. Hwang, D. Ahn, A spice-compatible new silicon nanowire field-effect transistors (snwfets) model. IEEE Trans. Nanotechnol. **8**, 643–649 (2009)
26. H. Elhadidy, J. Sikula, J. Franc, Symmetrical current-voltage characteristic of a metal-semiconductor-metal structure of schottky contacts and parameter retrieval of a cdte structure. Semicond. Sci. Technol. **27**(1), 015006 (2012)
27. S. Lee et al., Equivalent circuit model of semiconductor nanowire diode by spice. J. Nanosci. Nanotechnol. (2007)
28. C.Y. Yim, et al., Electrical properties of the zno nanowire transistor and its analysis with equivalent circuit model. J. Korean Phys. Soc. **48**, 1565–1569 (2006)
29. K. Steiner, Capacitance-voltage measurements on schottky diodes with poor ohmic contacts. IEEE Trans. Instrum. Meas. **42**(1), 39–43 (1993)
30. M. Bleicher, E. Lange, Schottky-barrier capacitance measurements for deep level impurity determination. Solid State Electron. **16**(3), 375–380 (1973)
31. P.S. Ho, E.S. Yang, H.L. Evans, X. Wu, Electronic states at silicide-silicon interfaces. Phys. Rev. Lett. **56**(1), 177–180 (1986)
32. J. Werner, A.F.J. Levi, R.T. Tung, M. Anzlowar, M. Pinto, Origin of the excess capacitance at intimate schottky contacts. Phys. Rev. Lett. **60**(1), 53–56 (1988)
33. I. Tzouvadaki, N. Aliakbarinodehi, G. de Micheli, S. Carrara, The memristive effect as a novelty in drug monitoring. Nanoscale **9**(27), 9676–9684 (2017)
34. S. Shigdar, J. Lin, Y. Yu, M. Pastuovic, M. Wei, W. Duan, Rna aptamer against a cancer stem cell marker epithelial cell adhesion molecule. Cancer Sci. **102**(5), 991–998 (2011)
35. D.H.J. Bunka, P.G. Stockley, Aptamers come of age -at last. Nat. Rev. Microbiol. **4**(8), 588–596 (2006)
36. E. Levy-Nissenbaum, A.F. Radovic-Moreno, A.Z. Wang, R. Langer, O.C. Farokhzad, Nanotechnology and aptamers: applications in drug delivery. Trends Biotechnol. **26**(8), 442–449 (2008)
37. M. Souada, B. Piro, S. Reisberg, G. Anquetin, V. Noël, M. Pham, Label-free electrochemical detection of prostate-specific antigen based on nucleic acid aptamer. Biosens. Bioelectron. **68**, 49–54 (2015)
38. P. Jolly, N. Formisano, J. Tkáč, P. Kasák, C.G. Frost, P. Estrela, Label-free impedimetric aptasensor with antifouling surface chemistry: a prostate specific antigen case study. Sens. Actuators B Chem. **209**, 306–312 (2015)

39. B. Liu, L. Lu, E. Hua, S. Jiang, G. Xie, Detection of the human prostate-specific antigen using an aptasensor with gold nanoparticles encapsulated by graphitized mesoporous carbon. Microchim. Acta **178**(1), 163–170 (2012)
40. B. Kavosi, A. Salimi, R. Hallaj, F. Moradi, Ultrasensitive electrochemical immunosensor for psa biomarker detection in prostate cancer cells using gold nanoparticles/pamam dendrimer loaded with enzyme linked aptamer as integrated triple signal amplification strategy. Biosens. Bioelectron. **74**, 915–923 (2015)
41. Z. Yang, B. Kasprzyk-Hordern, S. Goggins, C.G. Frost, P. Estrela, A novel immobilization strategy for electrochemical detection of cancer biomarkers: DNA-directed immobilization of aptamer sensors for sensitive detection of prostate specific antigens. Analyst **140**(8), 2628–2633 (2015)
42. P. Jolly, V. Tamboli, R.L. Harniman, P. Estrela, C.J. Allender, J.L. Bowen, Aptamer-mip hybrid receptor for highly sensitive electrochemical detection of prostate specific antigen. Biosens. Bioelectron. **75**, 188–195 (2016)
43. K. Radhapyari, P. Kotoky, M.R. Das, R. Khan, Graphene-polyaniline nanocomposite based biosensor for detection of antimalarial drug artesunate in pharmaceutical formulation and biological fluids. Talanta **111**, 47–53 (2013)
44. B. Bo, X. Zhu, P. Miao, D. Pei, B. Jiang, Y. Lou, Y. Shu, G. Li, An electrochemical biosensor for clenbuterol detection and pharmacokinetics investigation. Talanta **113**(9), 36–40 (2013)
45. D.-M. Kim, M.A. Rahman, M.H. Do, C. Ban, Y.-B. Shim, An amperometric chloramphenicol immunosensor based on cadmium sulfide nanoparticles modified-dendrimer bonded conducting polymer. Biosens. Bioelectron. **25**(3), 1781–1788 (2010)
46. W.U. Wang, C. Chen, K.-H. Lin, Y. Fang, C.M. Lieber, Label-free detection of small-molecule-protein interactions by using nanowire nanosensors. Proc. Natl. Acad. Sci. USA **102**(3), 3208–3212 (2005)
47. H. Karimi-Maleh, F. Tahernejad-Javazmi, N. Atar, M.L. Yola, V.K. Gupta, A.A. Ensafi, A novel DNA biosensor based on a pencil graphite electrode modified with polypyrrole/functionalized multiwalled carbon nanotubes for determination of 6-mercaptopurine anticancer drug. Ind. Eng. Chem. Res. **54**(4), 3634–3639 (2015)
48. R.N. Goyal, V.K. Gupta, S. Chatterjee, Voltammetric biosensors for the determination of paracetamol at carbon nanotube modified pyrolytic graphite electrode. Sens. Actuators B Chem. **149**(8), 252–258 (2010)
49. Ľ. Švorc, J. Sochr, P. Tomčík, M. Rievaj, D. Bustin, Simultaneous determination of paracetamol and penicillin V by square-wave voltammetry at a bare boron-doped diamond electrode. Electrochim. Acta 68(4), 227–234 (2012)
50. K. Radhapyari, P. Kotoky, R. Khan, Detection of anticancer drug tamoxifen using biosensor based on polyaniline probe modified with horseradish peroxidase. Mater. Sci. Eng. C Mater. Biol. Appl. **33**, 583–587 (2013)
51. M.N. Kammer, I.R. Olmsted, A.K. Kussrow, M.J. Morris, G.W. Jackson, D.J. Bornhop, Characterizing aptamer small molecule interactions with backscattering interferometry. Analyst **139**, 5879–5884 (2014)
52. M. Simiele, C. Carcieri, A. De Nicolò, A. Ariaudo, M. Sciandra, A. Calcagno, S. Bonora, G. Di Perri, A. D'Avolio, A LC-MS method to quantify tenofovir urinary concentrations in treated patients. J. Pharm. Biomed. Anal. **114**(10), 8–11 (2015)
53. R. Jain, R. Sharma, Cathodic adsorptive stripping voltammetric detection and quantification of the antiretroviral drug tenofovir in human plasma and a tablet formulation. J. Electrochem. Soc. **160**(8), H489–H493 (2013)
54. M.E. Barkil, M.-C. Gagnieu, J. Guitton, Relevance of a combined uv and single mass spectrometry detection for the determination of tenofovir in human plasma by hplc in therapeutic drug monitoring. J. Chromatogr. B **854**(7), 192–197 (2007)